



Food Starch Structure Impacts Gut Microbiome Composition

 Frederick J. Warren,^{a*} Naoki M. Fukuma,^{b,c,d*} Deirdre Mikkelsen,^{a,e} Bernadine M. Flanagan,^{a,e} Barbara A. Williams,^{a,e} Allan T. Lisle,^f Páiraic Ó Cuív,^{b,c} Mark Morrison,^{b,c} Michael J. Gidley^{a,f}

^aCentre for Nutrition and Food Sciences, Queensland Alliance for Agriculture and Food Innovation, The University of Queensland, St. Lucia, Brisbane, Queensland, Australia

^bDiamantina Institute, Faculty of Medicine, The University of Queensland, Woolloongabba, Brisbane, Queensland, Australia

^cTranslational Research Institute, The University of Queensland, Woolloongabba, Brisbane, Queensland, Australia

^dResearch Faculty of Agriculture, Hokkaido University, Sapporo, Japan

^eARC Centre of Excellence in Plant Cell Walls, Centre for Nutrition and Food Sciences, Queensland Alliance for Agriculture and Food Innovation, The University of Queensland, St. Lucia, Brisbane, Queensland, Australia

^fSchool of Agriculture and Food Sciences, The University of Queensland, Gatton, Queensland, Australia

ABSTRACT Starch is a major source of energy in the human diet and is consumed in diverse forms. Resistant starch (RS) escapes small intestinal digestion and is fermented in the colon by the resident microbiota, with beneficial impacts on colonic function and host health, but the impacts of the micro- and nanoscale structure of different physical forms of food starch on the broader microbial community have not been described previously. Here, we use a porcine *in vitro* fermentation model to establish that starch structure dramatically impacts microbiome composition, including the key amylolytic species, and markedly alters both digestion kinetics and fermentation outcomes. We show that three characteristic food forms of starch that survive digestion in the small intestine each give rise to substantial and distinct changes in the microbiome and in fermentation products. Our results highlight the complexity of starch fermentation processes and indicate that not all forms of RS in foods are degraded or fermented in the same way. This work points the way for the design of RS with tailored degradation by defined microbial communities, informed by an understanding of how substrate structure influences the gut microbiome, to improve nutritive value and/or health benefits.

IMPORTANCE Dietary starch is a major component in the human diet. A proportion of the starch in our diet escapes digestion in the small intestine and is fermented in the colon. In this study, we use a model of the colon, seeded with porcine feces, in which we investigate the fermentation of a variety of starches with structures typical of those found in foods. We show that the microbial community changes over time in our model colon are highly dependent on the structure of the substrate and how accessible the starch is to colonic microbes. These findings have important implications for how we classify starches reaching the colon and for the design of foods with improved nutritional properties.

KEYWORDS carbohydrate structure, fermentation, microbial ecology, resistant starch, short-chain fatty acids

Many gut bacteria are known to degrade and/or ferment starch (1). The starch uptake system (*sus*) of *Bacteroides thetaiotaomicron* serves as the progenote model of the polysaccharide utilization loci (PUL) across the *Bacteroidetes* phylum, and more recently, the “amylosome” multiprotein complexes of the Gram-positive *Firmicutes* bacterium *Ruminococcus bromii* have been characterized (2–4). Other commensal

Received 14 February 2018 Accepted 21 April 2018 Published 16 May 2018

Citation Warren FJ, Fukuma NM, Mikkelsen D, Flanagan BM, Williams BA, Lisle AT, Ó Cuív P, Morrison M, Gidley MJ. 2018. Food starch structure impacts gut microbiome composition. *mSphere* 3:e00086-18. <https://doi.org/10.1128/mSphere.00086-18>.


Editor Garret Suen, University of Wisconsin—Madison

Copyright © 2018 Warren et al. This is an open-access article distributed under the terms of the [Creative Commons Attribution 4.0 International license](https://creativecommons.org/licenses/by/4.0/).

Address correspondence to Mark Morrison, m.morrison1@uq.edu.au, or Michael J. Gidley, m.gidley@uq.edu.au.

* Present address: Frederick J. Warren, Quadram Institute Biosciences, Norwich, United Kingdom; Naoki M. Fukuma, Obihiro University of Agriculture and Veterinary Medicine, Obihiro, Japan.

F.J.W. and N.M.F. contributed equally to this article.

 Starch structure impacts microbiome composition in *in vitro* models. [@starchlabs](https://twitter.com/starchlabs)

bacteria widely recognized for their beneficial effects on human health, such as *Eubacterium rectale* and *Faecalibacterium prausnitzii* can utilize the maltodextrins released by these degradative bacteria to support their growth (5–8).

Several structural features have been identified that can lead to starch escaping digestion in the small intestine (SI) and thereby being defined as resistant starch (RS) (5, 9, 10). These features include the following: (i) the native, semicrystalline (double-helical), granular form of starch, such as that found in raw foods, such as bananas; (ii) the partially recrystallized double-helical structures that form when starch is cooked and allowed to cool found, for example, in cold potatoes and stale bread; and (iii) starch which is encapsulated within matrices such as intact plant tissue or processed forms such as pasta, and therefore not available for digestion by small intestinal enzymes (11). It has been shown that starch from these materials is recovered from ileal effluents and therefore is available for fermentation in the colon (9, 12, 13).

In addition to our enhanced understanding of the role of specific gut microbiota, the positive effects from resistant starches on metabolic and cellular measures in human and animal studies have prompted a resurgent interest in their use to prevent and control digestive disorders and/or diseases, for example, improvements in insulin sensitivity which result from the effects of microbial metabolites produced during RS fermentation on secretion of gut peptides involved in appetite regulation and glucose homeostasis (14, 15). Furthermore, while it is known that starch structure can influence the ability of isolated bacterial species to ferment starch (5), there is limited understanding of how these properties affect temporal and/or spatial variations in the microbiome, as well as starch fermentation kinetics and characteristics.

Here, we examine how variations in food starch structure affect the gut microbiome, together with the kinetics of fermentation and the subsequent production of short-chain fatty acids (SCFA). We use a batch fermentation system inoculated with fecal microbiota from pigs fed a tightly controlled low-RS diet. This resulted in a fecal inoculum which was naive to RS prior to the start of the experiment, due to the low intake of RS in the pig's diet. Pigs have long been used as a model for the human digestive tract, as they are omnivorous and have similar organ structures and functions, and importantly, the gut microbiota of pigs is relatively similar to that of humans (16, 17).

By utilizing a wide range of physical structures of starch substrates, we drive reproducible changes in microbial community composition and fermentation kinetics. The samples analyzed included examples of the following: (i) starch encapsulated within plant tissue (sorghum grain tissue [ST], maize kernel tissue [MT], potato tuber tissue [PT], chickpea endosperm tissue [CT]) or processed food (pasta [PA]); (ii) the native granular form of starch (potato with and without prior amylase treatment; native potato starch [PS] and native potato starch [amylase digested] [PSA]); (iii) partially recrystallized starches from cook/cool treatments (potato and high-amylose maize with and without prior amylase treatment; cooked and recrystallized potato starch [PSC], PSC [amylase digested] [PSCA], cooked and recrystallized maize starch [MSC], and MSC [amylase digested] [MSCA]). These three forms of starch are commonly referred to as RS types I, II, and III, respectively, in the literature (11). The findings demonstrate that different starch substrates produce defined temporal changes in microbiome composition during fermentation. Three distinct microbial communities were identified dependent on substrate structure, which resulted in distinct fermentation kinetics and SCFA production profiles. The substrates giving rise to the three microbial communities did not correspond to the conventional structural definitions of RS and suggest a new classification of RS based on microbiota response.

RESULTS

Starch structure and interactions with microbiota during fermentation. We first examined the double-helical order present in the starch for each substrate, calculated from their ^{13}C cross-polarization magic angle spinning (CP/MAS) nuclear magnetic resonance (NMR) spectra (18). There was large variation in the helical order at the start

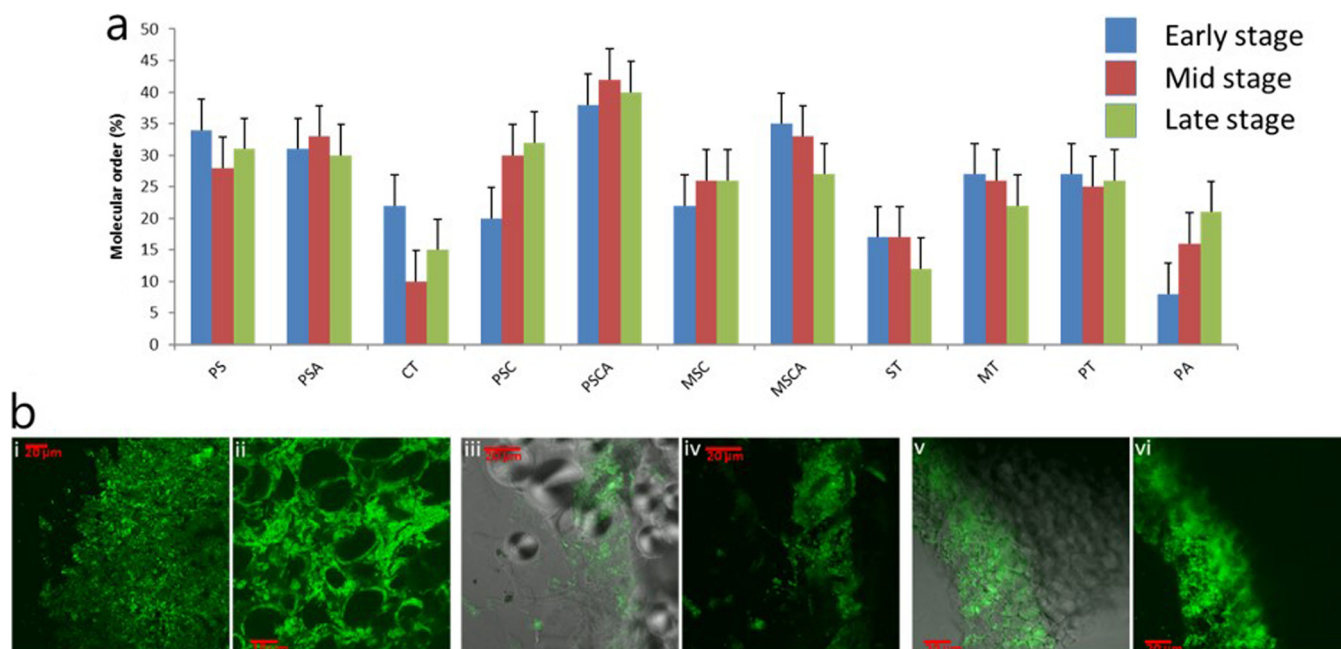


FIG 1 ^{13}C CP/MAS NMR analysis and microscopy of substrates. (a) Percentage double-helical order in starch substrates before fermentation (blue), during the exponential phase of fermentation (red) and at the endpoint of fermentation (green). (b) FISH visualization of the bacterial biofilms (green) associated with the nonstarch polysaccharide (NSP)-containing substrates pasta (i and ii), potato tissue (iii and iv), and maize tissue (v and vi) after 24 h of fermentation. Bacteria were hybridized with the EUB338Mix FITC probe.

of fermentation between the different substrates. However, only PSC and PA showed a significant change in molecular order with fermentation time, indicating that microbial amylolytic enzymes are able to attack crystalline and amorphous starch equally efficiently (Fig. 1a). Fermentations coupled to fluorescence *in situ* hybridization (FISH) using the universal bacterial probe mix and confocal laser scanning microscopy enabled visualization of the biofilms associated with food and plant tissue particulate substrates PA, PT, and MT, respectively, after 24 h of fermentation (Fig. 1b). It is evident that the microarchitecture of these substrates influenced bacterial access to starch within these substrates at this fermentation time point. For PA, the starch within the outer matrix of the strands is readily degraded, with no granular morphologies maintained (Fig. 1bi), while in the center of the PA strands, bacterial cells surround and begin to envelop the intact starch granules (Fig. 1bii). For PT, those starch granules encased within the fine cell wall matrices remain relatively intact, and the bacteria are primarily associated with the cell wall components. However, those granules free of the cell wall matrices are extensively decorated with a biofilm (Fig. 1biii and 1biv). For MT, the cell wall matrices appear to be more rigid and thicker than observed for PT, thereby limiting bacterial access primarily to those granules at the peripheral edges of the kernel (Fig. 1bv and 1bvi).

Temporal dynamics of microbiome composition during fermentation characterized by 16S rRNA gene amplicon sequencing. We identified 31 genera that comprised $\geq 0.5\%$ of the microbial communities across all substrates and fermentation time points (see Fig. S1 in the supplemental material). The distribution pattern of those genera was significantly different among the purified starches (Fig. S2) and tissue substrates (Fig. S3). The temporal distributions of these 31 genera throughout the fermentation time course were analyzed to generate a hierarchical clustering (Fig. 2a; see Data Set S1 for relative operational taxonomic unit [OTU] abundances). The 11 types of substrates clustered into three different microbial communities (MCs). Communities fermenting the cooked and cooled starches (PSC, PSCA, MSC, and MSCA) as well as PA clustered together and formed microbial community I (MC-I). MC-II comprised native potato starches (PS and PSA), CT, and PT. Microbial communities ferment-

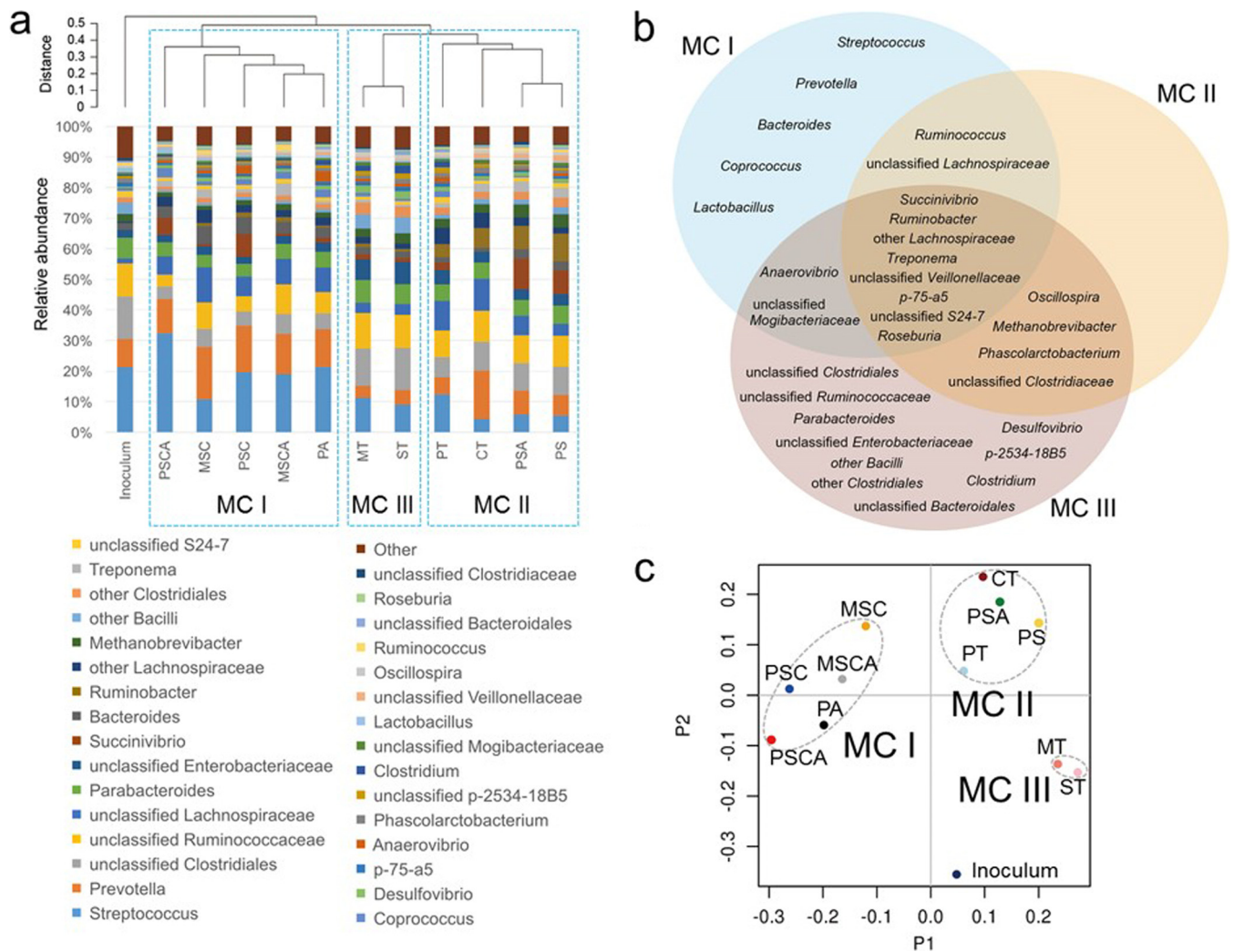


FIG 2 Starch substrates produce three distinct microbial community profiles during fermentation. (a) Compared to the starting inoculum, the communities could be subdivided into three microbial communities (MC; I, II, and III) based on hierarchical clustering of the genus distribution profiles produced from each substrate. (b) All three MCs share a relatively small core microbiome, and distinct genera can differentiate between the MC-I and MC-III profiles from MC-III ($P < 0.05$) abundance. (c) The PCoA plots of the communities produced for each substrate retained the overall clustering and were clearly separable from the starting inoculum. The substrate designations are the same as those described in the text.

ing MT and ST clustered together and formed MC-III (Fig. 2a). The MC-I microbiome included higher abundance of well-characterized gut bacterial genera, including *Streptococcus*, *Prevotella*, *Bacteroides*, *Coprococcus*, and *Lactobacillus*, while MC-III included higher abundance of *Parabacteroides*, *Desulfovibrio*, *Clostridium*, and several unclassified bacterial groups compared with other MCs. The MC-II formed an intermediate community between MC-I and MC-III (Fig. 2b). This clustering was confirmed by principal-coordinate analysis (PCoA) plotting (Fig. 2c).

These three MCs also showed differential kinetic shifts, represented by taxonomic distribution patterns as well as PCoA plottings (Fig. 3 and Fig. S1). MC-I showed rapid growth and predominance of *Streptococcus* in the first 6 h, resulting in depression of the community diversity, and both *Streptococcus* and *Prevotella* were the predominant genera throughout the fermentation. In MC-II, those two genera decreased by the middle of the fermentation period, with *Ruminobacter* gradually increasing and becoming dominant from 16 h to 30 h, followed by the dominance of *Succinivibrio* and/or unclassified *Lachnospiraceae* for the remainder of the fermentation. MC-III did not show a major community shift in the beginning and middle phases of fermentation, but after 48 h of incubation, unclassified *Clostridiales* and other *Bacillus* species became domi-

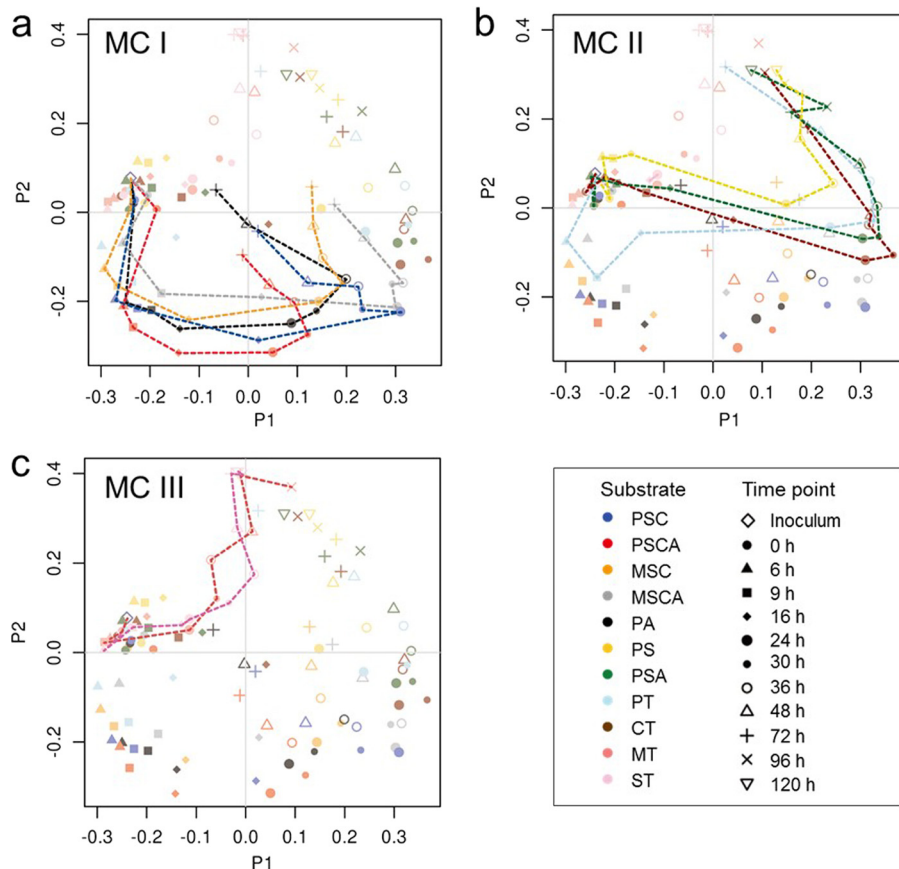


FIG 3 Microbial community dynamics for MC-I, MC-II, and MC-III are different. (a to c) The PCoA plots of the genus distribution profiles for individual samples collected at different time points during the fermentation of each substrate, with those substrates giving rise to the MC-I, MC-II, and MC-III profiles indicated by the dashed lines in panels a to c. Here, the profile of the starting inoculum is placed central to the samples collected from each substrate fermentation at 0 h, as indicated in each panel. Each substrate is color coded, and its designation is the same as those described in the text. Datum points for other substrates are included for reference.

nant groups, leading to a reduction in the diversity. PCoA based on a genus-level distribution showed that the microbiota composition from each of the MC groupings diverged throughout the time course of the experiment, from a similar initial condition (Fig. 3).

Functional properties inherent to the microbiomes present in the different fermentations were predicted using PICRUSt.

Profiles of the predicted genes annotated for carbohydrate metabolism also clustered fermentation substrates into the same three MCs (Fig. 4a). Of these clusters, MC-I possessed the highest inferred gene counts annotated for starch and sucrose metabolism and polysaccharide degradation and metabolism. This indicates that the PA, PSC, PSCA, MSC, and MSCA starches promoted highly amylolytic microbes, including *Streptococcus*, *Prevotella*, and *Bacteroides* in MC-I (as shown above). The detailed enzymatic profiles for carbohydrate degradation and transportation were investigated from the output of the PICRUSt analysis (Fig. 4b). Over the length of time of incubation, the MC-I is predicted to possess a greater variety of the major amylolytic enzymes, such as α -amylase, starch phosphorylase, and oligo-1,6-glucosidase, and these were less abundant in MC-II- and MC-III-driven fermentations. This corresponds to the relatively accessible but densely packed starch in the cooked, cooled starch and the cooked pasta samples which give rise to MC-I. In contrast, a greater variety of pectinolytic, xylanolytic, and cellulolytic enzymes were putatively identified in MC-II and MC-III. The enzyme profile for MC-III did not show a drastic kinetic shift, which corresponds well to the kinetics of the taxonomic

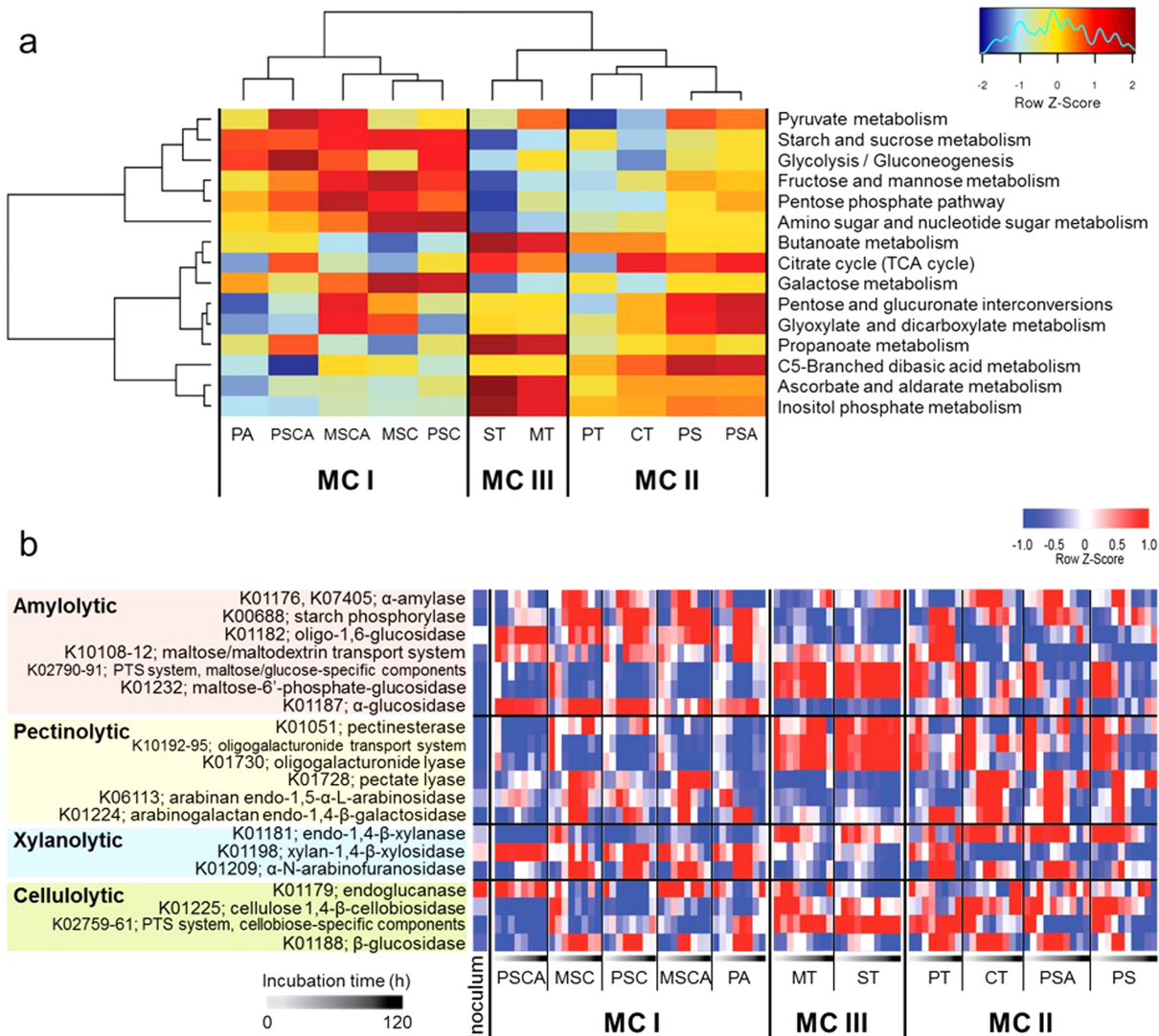


FIG 4 Dynamics of inferred gene abundance profiles for polysaccharide degradation and solute transport. Gene functions were predicted and quantified from the taxonomic profiles determined for the different substrate fermentations at each sampling time point using PICRUSt. (a) Distribution of genes present in pathways categorized in carbohydrate metabolism. TCA, tricarboxylic acid. (b) The heat map represents the Z-score change for each predicted gene relative to the mean abundance for each KEGG (Kyoto Encyclopedia of Genes and Genomes) gene group, calculated from all data combined.

distribution (Fig. S1). Several enzymes in the MC-II profiles showed time-specific patterns, where enzymes active on polysaccharides (pectinesterase, endo-1,4- β -xylanase, and cellulose 1,4- β -cellobiosidase) were detected in the early to middle stage of incubation, while those active on the degradation products or polysaccharide side chains (arabinogalactan endo-1,4- β -galactosidase, α -N-arabinofuranosidase, and β -glucosidase) were found in the middle to late incubation times. These outcomes suggest that the MC-II gradually degraded the nonstarch polysaccharides (pectin, cellulose, and hemicellulose) in the highly hydrated potato and chickpea tissues, whereas MC-III slowly and minimally broke down MT and ST starches encapsulated within the much more densely packed (less-hydrated) cereal grain tissues. Thus, the early stages of MC-II development followed those of MC-III because both involve cell wall degradation, with later stages of MC-II development being similar to MC-I where starch degradation predominates. The interesting nonconformers in this analysis are the native potato starch (with or without prior amylase treatment), which clustered with chickpea and potato tissue in MC-II, and the cooked, cooled potato starch (with or

TABLE 1 Kinetic parameters for gas production vary depending on substrate and microbial community^a

Microbial community and substrate or parameter ^b	DMCV (ml) ^c	$T_{R_{max}}$ (h)	R_{max} (ml/h)	$T_{1/2}$ (h)
MC-I	349 (4.2) A	19.5 (0.90) A	9.6 (0.19) A	31.9 (1.79) A
PSC	380 AB	17.3 CDE	11.4 AB	25.6 DE
PSCA	385 A	8.78 E	12.1 A	23.3 E
MSC	326 C	26.8 ABC	8.0 CDE	36.8 CDE
MSCA	340 BC	24.1 ABC	7.2 DE	45.8 C
PA	312 C	20.9 BCD	9.5 BC	28.1 CDE
MC-II	331 (4.6) B	27.8 (0.98) B	7.7 (0.21) B	36.6 (1.96) A
PS	312 C	32.9 A	5.9 E	43.1 CD
PSA	375 AB	29.4 AB	7.8 CDE	38.7 CDE
PT	311 C	19.4 CD	9.0 CD	28.2 CDE
CT	324 C	29.5 AB	8.0 CD	36. CDE
MC-III	218 (6.4) C	10.6 (1.39) C	2.7 (0.30) C	98.4 (2.77) B
MT	200 D	9.3 E	2.3 F	131.1 A
ST	236 D	11.9 DE	3.2 F	65.7 B
Prob-MC	<0.0001	<0.0001	<0.0001	<0.0001
Prob-sub(MC)	<0.0001	<0.0001	<0.0001	<0.0001
MSD*	44.3	9.6	2.09	19.05

^aThe substrates are purified starch substrates, analyzed by botanical origin, hydrothermal pretreatment, and α -amylase pretreatment, and substrates containing nonstarch components. Values indicated with different letters are significantly different ($P < 0.05$). The values for microbial communities I, II, and III are shown in boldface type.

^bProb-MC, probability—microbial community; Prob-sub(MC), probability—substrate (microbial community); MSD*, maximum standard deviation.

^cDMCV, dry matter cumulative gas production.

without prior amylase treatment) in MC-I. It may be that this reflects the presence of species specialized in degrading the incompletely gelatinized starch in the potato and chickpea tissue, rather than the presence of cell wall degraders.

Gas production kinetics and SCFA production directly relate to microbial community composition. For both the maximum rate of gas production (R_{max}) and the time at which this occurs ($T_{R_{max}}$), significant differences were observed between the different MC groupings, indicating that changing the physical structure of the substrate directly influenced fermentation behavior. MC-I and MC-II had more closely related gas production kinetics, with no significant difference in the overall half-time ($T_{1/2}$) of gas production, while MC-III showed slower fermentation and statistically different values for all gas kinetic parameters (Table 1). This reflects the microbial community composition results (Fig. 2a and c), showing that MC-II shared closer community characteristics with MC-I than MC-III. As expected, acetate was the main SCFA produced for all substrates, followed by propionate and smaller amounts of butyrate, with differences seen in their relative proportions, and that of the ratio of branched-chain to linear SCFA, depending on the substrate and MC (Table 2).

In MC-I and MC-II, a tight network was observed among *Streptococcus*, *Prevotella*, *Lactobacillus*, and *Bacteroides* (Fig. S4 and S5). For MC-III (Fig. S6), the companion consortia were strikingly different and included unclassified bacterial groups (*Clostridiales*, *Veillonellaceae*, and *Bacteroidales*) and strongly favored fermentation schemes resulting in acetate and butyrate, reflected in the significantly higher production of acetate and butyrate during the fermentation of MC-III substrates. In addition, for MC-III, there was an increased production of branched-chain fatty acids (Table 2), suggesting greater protein fermentation. Consistent with this, the starch in these fermentations was less degradable as judged by the lower SCFA levels.

Amylolytic activity can be identified in the cell-free medium. An increase in amylolytic activity during fermentation was found in the spent cell-free medium for several substrates, indicating the release of amylolytic enzymes from the microbiota as

TABLE 2 SCFA and ammonia production are dependent on substrate and microbial community composition^a

Microbial community and substrate or parameter	Concn (mmol/g [DM])									
	Acetic acid	Propionic acid	Butyric acid	Total SCFA	NH ₃	% AcTot	% PrTot	% BuTot	% BrChPpn	
MC-I	5.6 (0.071) A	3.7 (0.56) A	0.20 (0.003) B	11.8 (0.14) A	3.6 (0.05) B	47.4 (0.11) B	31.7 (0.21) A	1.7 (0.03) C	0.203 (0.002) C	
PSC	5.6 BC	4.3 AB	0.20 ABC	12.3 B	3.9 BC	45.2 F	35.1 A	1.6 EF	0.170 AB	
PSCA	7.5 A	4.6 A	0.19 ABC	14.3 A	4.1 BCD	52.5 A	32.2 BC	1.4 F	0.149 A	
MSC	5.3 BCD	3.4 DE	0.21 AB	11.2 BC	4.3 CD	47.3 DE	29.9 CD	1.9 CDE	0.202 CD	
MSCA	5.3 BCD	3.4 CDE	0.21 AB	10.6 BCD	3.9 B	49.6 C	32.1 BC	2.0 CD	0.180 ABC	
PA	4.4 DEF	3.0 EF	0.17 C	10.2 CD	2.0 A	42.7 G	29.3 D	1.7 DE	0.313 F	
MC-II	4.9 (0.11) B	3.4 (0.89) B	0.21 (0.005) A	10.5 (0.22) B	3.9 (0.08) A	46.5 (0.18) C	32.5 (0.34) A	2.0 (0.04) B	0.220 (0.004) B	
PS	4.5 DEF	3.1 CDEF	0.22 A	9.9 CD	4.6 D	45.5 F	33.2 AB	2.3 BC	0.198 BCD	
PSA	6.2 B	4.2 ABC	0.21 ABC	12.6 AB	4.1 BCD	48.9 CD	33.2 AB	1.6 DEF	0.179 ABC	
PT	4.1 EF	2.7 F	0.19 ABC	8.9 D	1.9 A	45.9 F	30.5 BCD	2.1 C	0.268 E	
CT	4.9 BCD	3.5 BCD	0.23 A	10.7 BCD	4.8 D	45.7 EF	33.1 AB	2.1 BC	0.234 D	
MC-III	3.2 (0.18) C	1.5 (0.14) C	0.17 (0.007) C	6.3 (0.34) C	4.0 (0.12) A	51.0 (0.27) A	23.2 (0.52) B	2.6 (0.06) A	0.330 (0.005) A	
MT	3.0 FG	1.4 E	0.16 C	5.9 E	4.0 BCD	51.6 AB	23.5 E	2.7 A	0.377 G	
ST	3.4 FG	1.5 E	0.17 BC	6.7 E	3.9 BCD	50.5 BC	22.8 E	2.5 AB	0.283 EF	
Prob-MC	<0.0001	<0.0001	0.0003	<0.0001	0.0001	<0.0001	<0.0001	<0.0001	<0.0001	
Prob-sub(MC)	<0.0001	<0.0001	0.0011	<0.0001	<0.0001	<0.0001	<0.0001	<0.0001	<0.0001	

^aThe SCFA and ammonia products were analyzed by botanical origin, hydrothermal pretreatment and α -amylase pretreatment, and for substrates containing nonstarch components. Values indicated with different letters are significantly different ($P < 0.05$). The values for microbial communities I, II, and III are shown in boldface type. Abbreviations: DM, dry matter; AcTot, acetic acid total; PrTot, propionic acid total; BuTot, butyric acid total; BrChPpn, branched-chain fatty acid proportion; Prob-MC, probability—microbial community; Prob-sub(MC), probability—substrate (microbial community).

the starch was fermented (Fig. S7a to d). To explore whether the same structural features that limit small intestinal α -amylase digestion also affect microbial digestion kinetics, *in vitro* digestion experiments of starches with and without α -amylase pretreatment were carried out (Fig. S7e and f). While the starches more slowly digested by α -amylase were among those more slowly fermented by the microbiota, the trend was not statistically significant ($r^2 = 0.319$; $P = 0.113$), suggesting that different factors are limiting to gut microbiota fermentation of starch than small intestinal fermentation; for example, the microbiota can degrade cell walls which would inhibit starch digestion in the small intestine, and the microbiota possess a wider range of amylolytic enzymes, which may be better able to degrade more crystalline starch. Evidence for this is also shown in Fig. 1a, which shows that crystalline and amorphous starch was degraded at the same rate during fermentation.

DISCUSSION

Identifying differences in microbial community composition linked to differences in end products from the fermentation of starches with different physical structures is a key step toward the rational design of foods containing resistant starches to provide targeted health benefits. Our results indicate that microbial community composition is linked to substrate structure (Fig. 2) (5, 19–22). This variability can be explored and understood only through the use of starches with highly characterized structures, representing a broad range of different physical forms of starch, differing in structure at the macro-, micro-, and nanolength scales (23, 24). Given the large differences in fermentation patterns observed in the present study, we can also expect that large differences exist when starch is fermented by the human gut microbiota (both *in vitro* and *in vivo*). Our findings reveal how starch structure not only affects the kinetics of starch fermentation but also the structure-function relationships and ecological succession of the microbiome that develops during this process, reflecting changes in microbiome composition observed in *in vivo* feeding experiments in both humans and swine (5, 24, 25).

Defined changes in microbial community in swine fed resistant starch have been observed in a number of feeding studies in pigs. Umu et al. fed pigs retrograded starch and observed increases in *Prevotella*, *Lachnospiraceae*, and *Ruminococcus*, consistent with our findings for MC-I starches (including all retrograded starch substrates) (24). Sun et al. fed pigs raw potato starch (equivalent to PS, an MC-II starch), and described a

decrease in *Clostridium*, *Treponema*, *Oscillospira*, *Phascolarctobacterium*, RC9, and S24-7 and an increase in *Turicibacter*, *Blautia*, *Ruminococcus*, *Coprococcus*, and *Marvinbryantia* (26, 27). Many of these OTUs were also observed to show population shifts in MC-II in the *in vitro* experiments shown in this paper, for example *Clostridium*, *Treponema*, *Oscillospira*, *Phascolarctobacterium*, S24-7, and *Ruminococcus*. The time course results available using *in vitro* models add valuable additional information, for example showing that *Clostridium*, S24-7, and *Ruminococcus* are prevalent during the early stages of starch fermentation, but populations then drop during later stages of fermentation, when samples would be taken for *in vivo* experiments. The results shown here identify many similar OTUs to those seen *in vivo* but provide more detailed time course data and allow analysis across a wider range of substrates.

Identifying how different starches are fermented will allow for the design of foods containing resistant starch that drive potentially beneficial changes in gut microbiota (28, 29). It will also allow the identification of potentially less favorable forms of resistant starch. For instance, highly active amylolytic bacteria, such as *Bacteroides vulgatus* and *Streptococcus bovis*, and species whose populations have been shown to increase in response to diets rich in RS, such as *Prevotella copri* and *Ruminococcus gnavus*, are recognized to be associated with colorectal neoplasia (30), new onset rheumatoid arthritis (31), and pouchitis following colectomy in ulcerative colitis (UC) patients (32). In that context, many forms of colorectal cancer and ulcerative colitis principally arise in the distal colon and/or rectum, at which sites the microbiota may have been “preset” by the structural properties of the starch entering the large bowel. The large bowel operates much like a plug-flow digester, and the limited mixing of material means the resident microbiome that colonizes and matures with the food matrix does so under batch or fed-batch conditions (33). For these reasons, a time course assessment of the microbiome changes during batch fermentations, as conducted in the present study, offers insights not readily achievable from the small animal and clinical studies performed with different starches and/or foods thus far (7). The present work based on 16S rRNA sequencing is able to identify clear differences at the genus level during the time course of starch fermentation. Future work should aim to identify whether specific species with known disease associations are selected for by starches with defined structures to identify potential disease associations.

Our work highlights how the structural properties of the substrate can drive functional differences across the microbiome and points the way for the design of starch-containing foods with defined microbial communities and fermentation characteristics, as well as suggesting novel approaches to classifying RS on the functional basis of its fermentation pathway by the colonic microbiota.

MATERIALS AND METHODS

Substrates. Native potato starch (catalog no. S4251; Sigma-Aldrich, St. Louis, MO) and Gelose 80 high-amylose maize starch (Penford Australia Ltd., Sydney, Australia) were obtained commercially. Maize kernels (cv. Pioneer) were a gift from Glen Fox (University of Queensland, Brisbane, Australia), white sorghum kernels (cv. QL12) were a gift from Ian Godwin (University of Queensland, Brisbane, Australia), and separated chickpea cells were a gift from Sushil Dhital (University of Queensland, Brisbane, Australia). Potatoes (cv. Mozart) and pasta (Barilla no. 5; Barilla S.p.A, Parma, Italy) were purchased from a local supermarket (Brisbane, Australia).

From the native potato starch and maize starch, cooked and cooled starches were prepared by boiling 25 g of starch in 250 ml of deionized water (dH₂O) for 20 min. This was then cooled and stored in a fridge for 24 h to allow (partial) recrystallization. The resultant gel was then frozen at -80°C before freeze drying and grinding to a powder to produce cooked, cooled potato starch and maize starch, respectively. α -Amylase predigestion was conducted on selected substrates; native potato starch, cooked and cooled potato starch, and cooked and cooled maize starch following a modification of the INFOGEST protocol (34). Briefly, 7 g of starch was dispersed in 70 ml of phosphate-buffered saline (PBS) (catalog no. P4417; Sigma-Aldrich) containing 200 U/ml of porcine pancreatic α -amylase (E-PANAA; Megazyme, Bray, Ireland) and incubated at 37°C for 2 h with regular mixing by inversion. After 2 h, the reaction was stopped immediately by the addition of an equal volume of 0.3 M Na₂CO₃ (35). Samples were then centrifuged (2,000 \times g, 5 min) and washed in dH₂O three times, before washing the samples with ethanol and drying them by rotary evaporation.

Maize and sorghum kernels were prepared by soaking the kernels in excess dH₂O overnight before rinsing and boiling in dH₂O (20 g of kernel per 100 ml of water) for 1 h. After cooking, the kernels were

halved (sorghum) or quartered (maize). Potato was prepared by cutting the potato into 5-mm cubes and cooking the potato cubes in dH₂O (20 g in 200 ml) at 70°C for 5 min to achieve starch gelatinization while retaining intact cell walls (36). Pasta was prepared following the manufacturer's instructions. The pasta was broken into 1-cm lengths and boiled in dH₂O (20 g of pasta to 200 ml of water) for 8 min.

Dry matter content for the substrates was determined by oven drying in preweighed porcelain crucibles at 105°C for 24 h. Total starch content was determined using the Megazyme total starch assay (K-TSTA; Megazyme, Bray, Ireland). All substrates were prepared freshly and weighed in clean serum bottles. Native potato starch, amylase-treated native potato starch, cooked and cooled potato and maize starches, and amylase-treated, cooked, cooled maize and potato starches had 0.2 g (dry weight) weighed into 50-ml fermentation bottles. Maize and sorghum kernels, chickpeas, pasta, and potato had 0.5 g (dry weight) weighed in 100-ml fermentation bottles. All the fresh cooked samples (maize and sorghum kernels, chickpeas, pasta, and potato) were weighed out 24 h prior to the start of the experiment and kept refrigerated, with regular CO₂ sparging.

In vitro starch digestion kinetics. Substrates (100 mg [dry weight]) were weighed in 15-ml polypropylene tubes, to which 10 ml of phosphate-buffered saline (pH 7.2) was added and incubated at 37°C. At 0 min, porcine pancreatic α -amylase (E-PANAA; Megazyme, Bray, Ireland) was added to give 200-U/ml enzyme activity. Aliquots (100- μ l aliquots) were taken at defined time points up to 180 min and added to 100 μ l of 0.3 M Na₂CO₃ to stop the reaction. Reducing sugar production was measured using the 4-hydroxybenzoic acid hydrazide (PAHBAH) method of Lever (37) as described by Moretti and Thorson (38), using maltose standards. Absorbance was read using a Fluostar Optima plate reader (BMG Labtech, Morington, Australia) at a wavelength of 405 nm. Kinetic parameters were determined using the logarithm of slope (LOS) method (39, 40).

Collection and preparation of the inoculum. Porcine feces were collected from five Large White grower pigs of 30 to 40 kg. The pigs had been fed a semipurified diet consisting mainly of rapidly digestible maize starch and fishmeal for 10 days prior to fecal collection. This diet was formulated to contain low levels of nonstarch polysaccharide, and a highly digestible starch that is rapidly and completely digested in the small intestine (SI), avoiding possible adaptation of the large intestinal microbiota to any of the substrates tested. Feces were collected per rectum with a gloved finger and placed immediately into a warmed vacuum flask previously flushed with CO₂. The feces from all animals were combined and diluted 1:5 with prewarmed, sterile saline (0.9% NaCl). This mixture was mixed for 60 s using a handheld blender, and filtered through four layers of muslin cloth. All procedures were carried out under a constant stream of CO₂.

Batch fermentation and sampling. Fermentation experiments were performed by the method of Williams et al. (41). Briefly, samples were inoculated with 2.5 ml (50-ml fermentation bottles) or 5 ml (100-ml fermentation bottles) of diluted and homogenized pig fecal inoculum, and the resulting samples were fermented at 39°C for up to 146 h (depending on the fermentation rate of the substrate). At a series of time points throughout fermentation, duplicate bottles were plunged into an ice-water bath for 20 min to halt bacterial activity and then opened for sampling. After the pH of the fermentation fluid was measured, samples were taken for short-chain fatty acid (SCFA) and NH₃ analyses, as well as 500 μ l of fluid for analysis of amylase activity, which was immediately frozen in liquid nitrogen (LN₂). The remaining fermentation fluid was then centrifuged in a refrigerated centrifuge (4°C, 2,500 \times g, 5 min), and samples of biomass were taken and frozen in LN₂ for DNA extraction. The remaining biomass was frozen at -20°C and freeze-dried for ¹³C cross-polarization magic angle spinning (CP/MAS) nuclear magnetic resonance (NMR) analysis. Up to 25 gas readings were taken over a period of up to 146 h. Five replicates were used for determining gas kinetics. Substrate-free blanks were also prepared in duplicate for both the large and small bottles.

¹³C CP/MAS NMR. The freeze-dried fermentation biomass from different time points was studied using solid-state ¹³C CP/MAS NMR at a ¹³C frequency of 75.46 MHz on a Bruker MSL-300 spectrometer (Bruker, Billerica, MA, USA). The powder was packed in 4-mm-diameter, cylindrical, PSZ (partially stabilized zirconium-oxide) tubes with a Kelf endcap. The rotor was spun at 5 kHz at the magic angle (54.7°). The 90° pulse width was 5 μ s, and a contact time of 1 ms was used for all samples with a recycle delay of 3 s. Other parameters were set as follows: spectral width, 38 kHz; acquisition time, 50 ms; time domain points, 2,000; transform size, 4,000; line broadening, 50 Hz. At least 2,400 scans were accumulated for each spectrum. Spectra were referenced to external adamantane. Molecular order values were obtained through fitting to a published multivariate analysis tool (18).

FISH. After 24 h of fermentation, residual potato tuber tissue (PT), pasta (PA), and maize kernel tissue (MT) substrates were handled with forceps, gently placed into 5 ml of prealiquoted 4% paraformaldehyde (PFA) fixative, and incubated at 4°C overnight. Thereafter, the PFA fixative was discarded, and the samples were washed to remove any residual fixative. The fixed samples were stored in equal volumes of 1 \times PBS and 100% ethanol solution at -20°C until processed.

Prior to fluorescence *in situ* hybridization (FISH), samples were sectioned using a Cryostat Microm HM5650 instrument to prepare 50- μ m-thick sections. These sections were placed on slides which were coated with agarose to prevent loss of sample during hybridization. The slides were dehydrated and FISH was performed by the method of Gorham et al. (42). The universal bacterial probes EUB338, Eub338 II, and EUB338 III, labeled with fluorescein isothiocyanate (FITC), were combined as previously described (43) to form an equimolar mix for subsequent use.

DNA extraction and sequencing. Biomass from the 500- μ l aliquots of each fermentation sample was concentrated by centrifugation (16,000 \times g, 4°C, 5 min), and lysed by the RBB + C method (44). Total genomic DNA was extracted and purified using the Maxwell 16 LEV blood DNA kit (Promega, Madison, WI) and the Maxwell 16 MDx research instrument (Promega, Madison, WI) according to the manufac-

turer's instructions. The concentration and purity of genomic DNA were evaluated with the NanoDrop Lite spectrophotometer (Thermo Fisher Scientific, Waltham, MA). The variable regions V6 to V8 of the 16S rRNA gene were amplified from the purified DNA. The primers used in this study consisted of the Illumina primer overhang adapters and bacterial universal primers as follows: the forward overhang adapter and primer 926F (5'-TCG TCG GCA GCG TCA GAT GTG TAT AAG AGA CAG AAA CTY AAA KGA ATT GRC GG-3') and the reverse overhang adapter and primer 1392R (5'-GTC TCG TGG GCT CGG AGA TGT GTA TAA GAG ACA GAC GGG CGG TGW GTR C-3'). Dual-index barcodes were added to the amplicon target using the Nextera XT Index kit (Illumina, San Diego, CA). The concentrations of PCR product were measured by a Quantifluor double-stranded DNA (dsDNA) system (Promega, Madison, WI), and all PCR products were pooled into one tube in equal amounts. Paired-end sequencing was performed using the Illumina MiSeq platform (Illumina, San Diego, CA), supported and operated by the Australian Centre for Ecogenomics (Brisbane, Australia).

Analysis of 16S rRNA gene sequences. The raw 16S rRNA gene sequence data were analyzed by Quantitative Insight Into Microbial Ecology (QIIME) version 1.9.1 (45). Sequences with a Phred score of lower than 20 were removed. Chimeric sequences were checked and removed using USEARCH version 6.1.544 (46). The remaining high-quality reads were clustered into operational taxonomic units (OTUs) by PyNAST (47) with a 97% sequence identity threshold against the Greengenes core set database version 13.8 (48). The generated biome table was normalized using an equal subsampling size of 2,938 sequences. Distances between bacterial communities in different samples were calculated by the weighted UniFrac distance metric (49) in QIIME. Calypso (50) version 5.2 was used to generate hierarchical clustering, principal-coordinate analysis (PCoA) plots, and microbial network maps. Metagenomic function was predicted using PICRUSt (51) online Galaxy version by the method of Umu et al. (24). Heat maps were generated using Calypso and gplots package in R.

The White's nonparametric *t* test and Kruskal-Wallis *H* test were performed to compare the relative abundance of genera for two groups and more than three groups, respectively. Statistical significance was analyzed by Prism version 6.0g (GraphPad Software, La Jolla, CA). A *P* value of less than 0.05 was regarded as statistically significant.

Gas production kinetic analysis. Gas production kinetics were modelled using a monophasic exponential model as follows (52):

$$G = A/[1(C/t)^B]$$

where *G* is cumulative gas produced (in milliliters) at time *t* (in hours), *A* is asymptotic gas production, *B* is the switching characteristic of the curve, *C* is the time at which half of the asymptotic value has been reached (in hours), and *t* is time (in hours). Model parameters were estimated for each bottle, by nonlinear least squares with the SAS (version 9.3) NLIN procedure.

Two further parameters may be calculated from the results of this fitted curve, R_{\max} which is the maximum rate of gas production; and $T_{R_{\max}}$ the time at which R_{\max} occurs:

$$R_{\max} = \frac{(A)(C^B)(B)(T_{R_{\max}}^{-B-1})}{[1 + (C^B)(T_{R_{\max}}^{-B})]^2}$$

$$T_{R_{\max}} = C \left(\frac{B-1}{B+1} \right)^{\frac{1}{B}}$$

For statistical analysis, the substrates were separated into two groups and analyzed separately. Group 1 contained complex substrates (chickpea cells, sorghum tissue, maize tissue, potato tissue, and pasta), and group 2 contained purified starches (native potato starch, cooked and cooled potato starch, and cooked and cooled maize starch with or without amylase treatment). Purified starches were further subdivided into cooked versus native, amylase-treated starch versus non-amylase-treated starch, and maize versus potato to identify systematic variations across the different substrates.

Analysis of variance was conducted on the gas production parameters using the GLM procedure (SAS 9.3 for Windows, Cary, NC, USA) with model terms for microbial community (MC) group and substrates nested within each group. Any significant differences between substrates and MC group as described above were tested using Tukey's studentized range test.

Measurement of fermentation products and amylolytic activity. SCFAs were analyzed by gas chromatography using a Shimadzu GC-17A instrument (Kyoto, Japan), fitted with a ZB-FFAP column (30 m by 0.53 mm) (J & W Scientific, USA). The temperatures were as follows: 180°C for the injector, 210°C for the detector, and 85°C for the column. The temperature was held initially for 4 min and then increased at 15°C/min until the temperature reached 200°C, which was held for 2 min. The carrier gas was helium at 5.0 ml/min, 67 kPa for 2 min, and then 1.8 kPa/min to 81 kPa. The internal standard was 4-methyl valeric acid. Using the SCFA concentrations, the branched-chain ratio (BCR) was calculated. This is the ratio of mainly branched-chain acids (including valeric acid) to the straight-chain acids. The former is associated with the metabolism of amino acids, and the latter is associated with the metabolism of carbohydrates. Samples were analyzed for SCFA concentrations at time points throughout the fermentation and also at time zero. The SCFA values at time zero (contributed from the starting medium and inoculum) were taken into account in the subsequent analysis.

Ammonia was analyzed using a method modified from reference 53. Briefly, ammonium was determined colorimetrically, utilizing the chemical reaction of ammonium ions (NH_4^+) with sodium salicylate and nitroprusside in a weakly alkaline buffer, at a wavelength of 650 nm, using a high-throughput sample analyzer (AU400 chemistry analyzer; Olympus, Tokyo, Japan).

Amylolytic activity of the fermentation fluid was determined following filtration through a 0.2- μm syringe filter using the Enzcheck Ultra α -amylase assay (Life Technologies, Mulgrave, Australia) as

directed by the manufacturer. Fluorescence was measured using a Fluostar Optima plate reader (BMG Labtech, Mornington, Australia) with an excitation wavelength of 460 nm and emission wavelength of 520 nm.

Data availability. Nucleotide sequence data reported in this study are available in the DDBJ Sequence Read Archive under the accession number [DRA006773](https://doi.org/10.1128/DRA006773).

SUPPLEMENTAL MATERIAL

Supplemental material for this article may be found at <https://doi.org/10.1128/mSphere.00086-18>.

FIG S1, DOCX file, 0.9 MB.

FIG S2, DOCX file, 0.2 MB.

FIG S3, DOCX file, 0.2 MB.

FIG S4, DOCX file, 0.3 MB.

FIG S5, DOCX file, 0.3 MB.

FIG S6, DOCX file, 0.3 MB.

FIG S7, DOCX file, 0.1 MB.

DATA SET S1, XLSX file, 0.01 MB.

ACKNOWLEDGMENTS

F.J.W. gratefully acknowledges the receipt of a University of Queensland Post-Doctoral Fellowship. We gratefully acknowledge the support provided by the University of Queensland Reginald Ferguson Fellowship in Gastroenterology to P.Ó.C. This research was supported by a University of Queensland CIEF grant. The Translational Research Institute is supported by a grant from the Australian Government.

The conception of the project and experimental design was carried out by F.J.W., M.J.G., D.M., B.A.W., P.Ó.C., and M.M. The experimental work was conducted by F.J.W., N.M.F., D.M., and B.A.W. NMR analysis was conducted by B.M.F. Data analysis was carried out by F.J.W., N.M.F., B.A.W., A.T.L., and P.Ó.C. All authors contributed to the preparation and submission of the manuscript.

REFERENCES

- El Kaoutari A, Armougom F, Gordon JI, Raoult D, Henrissat B. 2013. The abundance and variety of carbohydrate-active enzymes in the human gut microbiota. *Nat Rev Microbiol* 11:497–504. <https://doi.org/10.1038/nrmicro3050>.
- Reeves AR, D'Elia JN, Frias J, Salyers AA. 1996. A *Bacteroides thetaiotaomicron* outer membrane protein that is essential for utilization of maltooligosaccharides and starch. *J Bacteriol* 178:823–830. <https://doi.org/10.1128/jb.178.3.823-830.1996>.
- Reeves AR, Wang GR, Salyers AA. 1997. Characterization of four outer membrane proteins that play a role in utilization of starch by *Bacteroides thetaiotaomicron*. *J Bacteriol* 179:643–649. <https://doi.org/10.1128/jb.179.3.643-649.1997>.
- Ze X, Ben David Y, Laverde-Gomez JA, Dassa B, Sheridan PO, Duncan SH, Louis P, Henrissat B, Juge N, Koropatkin NM, Bayer EA, Flint HJ. 2015. Unique organization of extracellular amylases into amyloosomes in the resistant starch-utilizing human colonic Firmicutes bacterium *Ruminococcus bromii*. *mBio* 6:e01058-15. <https://doi.org/10.1128/mBio.01058-15>.
- Ze X, Duncan SH, Louis P, Flint HJ. 2012. *Ruminococcus bromii* is a keystone species for the degradation of resistant starch in the human colon. *ISME J* 6:1535–1543. <https://doi.org/10.1038/ismej.2012.4>.
- Kovatcheva-Datchary P, Egert M, Maathuis A, Rajilić-Stojanović M, De Graaf AA, Smidt H, De Vos WM, Venema K. 2009. Linking phylogenetic identities of bacteria to starch fermentation in an in vitro model of the large intestine by RNA-based stable isotope probing. *Environ Microbiol* 11:914–926. <https://doi.org/10.1111/j.1462-2920.2008.01815.x>.
- Walker AW, Ince J, Duncan SH, Webster LM, Holtrop G, Ze X, Brown D, Stares MD, Scott P, Bergerat A, Louis P, McIntosh F, Johnstone AM, Lobley GE, Parkhill J, Flint HJ. 2011. Dominant and diet-responsive groups of bacteria within the human colonic microbiota. *ISME J* 5:220–230. <https://doi.org/10.1038/ismej.2010.118>.
- Bonnema A, Kelly J, Ryan S, McKinnon H, Romero-Gonzalez R, Louis P, Bosscher D, Duncan S, Johnstone A, Flint H, Harrold J, Halford J, Shirazi-Beechey S. 2015. SATIN (satiety innovation) project: dietary supplementa-
- tion with type 3 resistant starch induces distinct changes in gut microbiota of overweight human volunteers. *FASEB J* 29(Suppl):744.2.
- Edwards CH, Grundy MM, Grassby T, Vasilopoulou D, Frost GS, Butterworth PJ, Berry SE, Sanderson J, Ellis PR. 2015. Manipulation of starch bioaccessibility in wheat endosperm to regulate starch digestion, postprandial glycemia, insulinemia, and gut hormone responses: a randomized controlled trial in healthy ileostomy participants. *Am J Clin Nutr* 102:791–800. <https://doi.org/10.3945/ajcn.114.106203>.
- Bird AR, Conlon MA, Christophersen CT, Topping DL. 2010. Resistant starch, large bowel fermentation and a broader perspective of prebiotics and probiotics. *Benefic Microbes* 1:423–431. <https://doi.org/10.3920/BM2010.0041>.
- Dhital S, Warren FJ, Butterworth PJ, Ellis PR, Gidley MJ. 2017. Mechanisms of starch digestion by α -amylase—structural basis for kinetic properties. *Crit Rev Food Sci Nutr* 57:875–892. <https://doi.org/10.1080/10408398.2014.922043>.
- Englyst HN, Kingman SM, Cummings JH. 1992. Classification and measurement of nutritionally important starch fractions. *Eur J Clin Nutr* 46:S33–S50.
- Silvester KR, Englyst HN, Cummings JH. 1995. Ileal recovery of starch from whole diets containing resistant starch measured in vitro and fermentation of ileal effluent. *Am J Clin Nutr* 62:403–411. <https://doi.org/10.1093/ajcn/62.2.403>.
- Birt DF, Boylston T, Hendrich S, Jane J-L, Hollis J, Li L, McClelland J, Moore S, Phillips GJ, Rowling M, Schalinske K, Scott MP, Whitley EM. 2013. Resistant starch: promise for improving human health. *Adv Nutr* 4:587–601. <https://doi.org/10.3945/an.113.004325>.
- Bindels LB, Walter J, Ramer-Tait AE. 2015. Resistant starches for the management of metabolic diseases. *Curr Opin Clin Nutr Metab Care* 18:559–565. <https://doi.org/10.1097/MCO.0000000000000223>.
- Guilloteau P, Zabielski R, Hammon HM, Metzges CC. 2010. Nutritional programming of gastrointestinal tract development. Is the pig a good

- model for man? *Nutr Res Rev* 23:4–22. <https://doi.org/10.1017/S0954422410000077>.
17. Heinrich SN, Mosenthin R, Weiss E. 2013. Use of pigs as a potential model for research into dietary modulation of the human gut microbiota. *Nutr Res Rev* 26:191–209. <https://doi.org/10.1017/S0954422413000152>.
 18. Flanagan BM, Gidley MJ, Warren FJ. 2015. Rapid quantification of starch molecular order through multivariate modelling of ¹³C CP/MAS NMR spectra. *Chem Commun* 51:14856–14858. <https://doi.org/10.1039/c5cc06144j>.
 19. Abell GC, Cooke CM, Bennett CN, Conlon MA, McOrist AL. 2008. Phylogenotypes related to *Ruminococcus bromii* are abundant in the large bowel of humans and increase in response to a diet high in resistant starch. *FEMS Microbiol Ecol* 66:505–515. <https://doi.org/10.1111/j.1574-6941.2008.00527.x>.
 20. Flint HJ, Scott KP, Duncan SH, Louis P, Forano E. 2012. Microbial degradation of complex carbohydrates in the gut. *Gut Microbes* 3:289–306. <https://doi.org/10.4161/gmic.19897>.
 21. Martínez I, Kim J, Duffy PR, Schlegel VL, Walter J. 2010. Resistant starches types 2 and 4 have differential effects on the composition of the fecal microbiota in human subjects. *PLoS One* 5:e15046. <https://doi.org/10.1371/journal.pone.0015046>.
 22. Salonen A, Lahti L, Salojärvi J, Holtrop G, Korpela K, Duncan SH, Date P, Farquharson F, Johnstone AM, Lobley GE, Louis P, Flint HJ, de Vos WM. 2014. Impact of diet and individual variation on intestinal microbiota composition and fermentation products in obese men. *ISME J* 8:2218–2230. <https://doi.org/10.1038/ismej.2014.63>.
 23. Warren FJ, Gidley MJ, Flanagan BM. 2016. Infrared spectroscopy as a tool to characterise starch ordered structure—a joint FTIR–ATR, NMR, XRD and DSC study. *Carbohydr Polym* 139:35–42. <https://doi.org/10.1016/j.carbpol.2015.11.066>.
 24. Umu ÖC, Frank JA, Fangel JU, Oostindjer M, da Silva CS, Bolhuis EJ, Bosch G, Willats WG, Pope PB, Diep DB. 2015. Resistant starch diet induces change in the swine microbiome and a predominance of beneficial bacterial populations. *Microbiome* 3:16. <https://doi.org/10.1186/s40168-015-0078-5>.
 25. Human Microbiome Project Consortium. 2012. Structure, function and diversity of the healthy human microbiome. *Nature* 486:207–214. <https://doi.org/10.1038/nature11234>.
 26. Sun Y, Zhou L, Fang L, Su Y, Zhu W. 2015. Responses in colonic microbial community and gene expression of pigs to a long-term high resistant starch diet. *Front Microbiol* 6:877. <https://doi.org/10.3389/fmicb.2015.00877>.
 27. Sun Y, Su Y, Zhu W. 2016. Microbiome-metabolome responses in the cecum and colon of pig to a high resistant starch diet. *Front Microbiol* 7:779. <https://doi.org/10.3389/fmicb.2016.00779>.
 28. Flint HJ. 2012. The impact of nutrition on the human microbiome. *Nutr Rev* 70:510–513. <https://doi.org/10.1111/j.1753-4887.2012.00499.x>.
 29. Kelly J, Ryan S, McKinnon H, Romero-Gonzalez R, Louis P, Bosscher D, Bonnema A, Gratz S, Duncan S, Johnstone A, Flint H, Harrold J, Halford J, Shirazi-Beechey S. 2015. Dietary supplementation with a type 3 resistant starch induces butyrate producing bacteria within the gut microbiota of human volunteers. *Appetite* 91:438. <https://doi.org/10.1016/j.appet.2015.04.038>.
 30. Krishnan S, Slick GD. 2014. *Streptococcus bovis* infection and colorectal neoplasia: a meta-analysis. *Colorectal Dis* 16:672–680. <https://doi.org/10.1111/codi.12662>.
 31. Scher JU, Sczesnak A, Longman RS, Segata N, Ubeda C, Bielski C, Rostron T, Cerundolo V, Pamer EG, Abramson SB, Huttenhower C, Littman DR. 2013. Expansion of intestinal *Prevotella copri* correlates with enhanced susceptibility to arthritis. *Elife* 2:e01202. <https://doi.org/10.7554/eLife.01202>.
 32. Noor SO, Ridgway K, Scovell L, Kemsley EK, Lund EK, Jamieson C, Johnson IT, Narbad A. 2010. Ulcerative colitis and irritable bowel patients exhibit distinct abnormalities of the gut microbiota. *BMC Gastroenterol* 10:134. <https://doi.org/10.1186/1471-230X-10-134>.
 33. Hume I, Sakaguchi E. 1991. Patterns of digesta flow and digestion in foregut and hindgut fermenters, p 427–451. *In* Tsuda T, Sasaki Y, Kawashima R (ed), *Physiological aspects of digestion and metabolism in ruminants*. Proceedings of the Seventh International Symposium on Ruminant Physiology. Academic Press, Ltd, London, United Kingdom.
 34. Minekus M, Almginger M, Alvito P, Ballance S, Bohn T, Bourlieu C, Carrière F, Boutrou R, Corredig M, Dupont D, Dufour C, Egger L, Golding M, Karakaya S, Kirkhus B, Le Feunteun S, Lesmes U, Macierzanka A, Mackie A, Marze S, McClements DJ, Ménard O, Recio I, Santos CN, Singh RP, Vegarud GE, Wickham MSJ, Weitschies W, Brodtkorb A. 2014. A standardised static in vitro digestion method suitable for food—an international consensus. *Food Funct* 5:1113–1124. <https://doi.org/10.1039/C3FO60702J>.
 35. Tahir R, Ellis PR, Butterworth PJ. 2010. The relation of physical properties of native starch granules to the kinetics of amylolysis catalysed by porcine pancreatic α -amylase. *Carbohydr Polym* 81:57–62. <https://doi.org/10.1016/j.carbpol.2010.01.055>.
 36. Ormerod A, Ralfs J, Jobling S, Gidley M. 2002. The influence of starch swelling on the material properties of cooked potatoes. *J Mater Sci* 37:1667–1673. <https://doi.org/10.1023/A:1014965202596>.
 37. Lever M. 1972. A new reaction for colorimetric determination of carbohydrates. *Anal Biochem* 47:273–279. [https://doi.org/10.1016/0003-2697\(72\)90301-6](https://doi.org/10.1016/0003-2697(72)90301-6).
 38. Moretti R, Thorson JS. 2008. A comparison of sugar indicators enables a universal high-throughput sugar-1-phosphate nucleotidyltransferase assay. *Anal Biochem* 377:251–258. <https://doi.org/10.1016/j.jab.2008.03.018>.
 39. Butterworth PJ, Warren FJ, Grassby T, Patel H, Ellis PR. 2012. Analysis of starch amylolysis using plots for first-order kinetics. *Carbohydr Polym* 87:2189–2197. <https://doi.org/10.1016/j.carbpol.2011.10.048>.
 40. Edwards CH, Warren FJ, Milligan PJ, Butterworth PJ, Ellis PR. 2014. A novel method for classifying starch digestion by modelling the amylolysis of plant foods using first-order enzyme kinetic principles. *Food Funct* 5:2751–2758. <https://doi.org/10.1039/C4FO00115J>.
 41. Williams BA, Bosch MW, Boer H, Versteegen MWA, Tamminga S. 2005. An in vitro batch culture method to assess potential fermentability of feed ingredients for monogastric diets. *Anim Feed Sci Technol* 123-124: 445–462. <https://doi.org/10.1016/j.anifeedsci.2005.04.031>.
 42. Gorham JB, Williams BA, Gidley MJ, Mikkelsen D. 2016. Visualization of microbe-dietary remnant interactions in digesta from pigs, by fluorescence in situ hybridization and staining methods; effects of a dietary arabinoxylan-rich wheat fraction. *Food Hydrocolloids* 52: 952–962. <https://doi.org/10.1016/j.foodhyd.2015.09.011>.
 43. Daims H, Brühl A, Amann R, Schleifer K-H, Wagner M. 1999. The domain-specific probe EUB338 is insufficient for the detection of all Bacteria: development and evaluation of a more comprehensive probe set. *Syst Appl Microbiol* 22: 434–444. [https://doi.org/10.1016/S0723-2020\(99\)80053-8](https://doi.org/10.1016/S0723-2020(99)80053-8).
 44. Yu Z, Morrison M. 2004. Improved extraction of PCR-quality community DNA from digesta and fecal samples. *Biotechniques* 36:808–812.
 45. Caporaso JG, Kuczynski J, Stombaugh J, Bittinger K, Bushman FD, Costello EK, Fierer N, Peña AG, Goodrich JK, Gordon JI, Huttley GA, Kelley ST, Knights D, Koenig JE, Ley RE, Lozupone CA, McDonald D, Muegge BD, Pirrung M, Reeder J, Sevinsky JR, Turnbaugh PJ, Walters WA, Widmann J, Yatsunenko T, Zaneveld J, Knight R. 2010. QIIME allows analysis of high-throughput community sequencing data. *Nat Methods* 7:335–336. <https://doi.org/10.1038/nmeth.f.303>.
 46. Edgar RC. 2010. Search and clustering orders of magnitude faster than BLAST. *Bioinformatics* 26:2460–2461. <https://doi.org/10.1093/bioinformatics/btq461>.
 47. Caporaso JG, Bittinger K, Bushman FD, DeSantis TZ, Andersen GL, Knight R. 2010. PyNAST: a flexible tool for aligning sequences to a template alignment. *Bioinformatics* 26:266–267. <https://doi.org/10.1093/bioinformatics/btp636>.
 48. DeSantis TZ, Hugenholtz P, Larsen N, Rojas M, Brodie EL, Keller K, Huber T, Dalevi D, Hu P, Andersen GL. 2006. Greengenes, a chimera-checked 16S rRNA gene database and workbench compatible with ARB. *Appl Environ Microbiol* 72:5069–5072. <https://doi.org/10.1128/AEM.03006-05>.
 49. Lozupone C, Knight R. 2005. UniFrac: a new phylogenetic method for comparing microbial communities. *Appl Environ Microbiol* 71: 8228–8235. <https://doi.org/10.1128/AEM.71.12.8228-8235.2005>.
 50. Zakrzewski M, Proietti C, Ellis JJ, Hasan S, Brion M-J, Berger B, Krause L. 2017. Calypso: a user-friendly web-server for mining and visualizing microbiome–environment interactions. *Bioinformatics* 33:782–783. <https://doi.org/10.1093/bioinformatics/btw725>.
 51. Langille MG, Zaneveld J, Caporaso JG, McDonald D, Knights D, Reyes JA, Clemente JC, Burkpile DE, Vega Thurber RL, Knight R, Beiko RG, Huttenhower C. 2013. Predictive functional profiling of microbial communities using 16S rRNA marker gene sequences. *Nat Biotechnol* 31: 814–821. <https://doi.org/10.1038/nbt.2676>.
 52. Groot JCI, Cone JW, Williams BA, Debersaques FMA, Lantinga EA. 1996. Multiphasic analysis of gas production kinetics for in vitro fermentation of ruminant feeds. *Anim Feed Sci Technol* 64:77–89. [https://doi.org/10.1016/S0377-8401\(96\)01012-7](https://doi.org/10.1016/S0377-8401(96)01012-7).
 53. Bolleter WT, Bushman CJ, Tidwell PW. 1961. Spectrophotometric determination of ammonia as indophenol. *Anal Chem* 33:592–594. <https://doi.org/10.1021/ac60172a034>.